# NJC

## Accepted Manuscript

This is an *Accepted Manuscript*, which has been through the Royal Society of Chemistry peer review process and has been accepted for publication.

*Accepted Manuscripts* are published online shortly after acceptance, before technical editing, formatting and proof reading. Using this free service, authors can make their results available to the community, in citable form, before we publish the edited article. We will replace this *Accepted Manuscript* with the edited and formatted *Advance Article* as soon as it is available.

You can find more information about *Accepted Manuscripts* in the **Information for Authors**.

Please note that technical editing may introduce minor changes to the text and/or graphics, which may alter content. The journal's standard **Terms & Conditions** and the **Ethical guidelines** still apply. In no event shall the Royal Society of Chemistry be held responsible for any errors or omissions in this *Accepted Manuscript* or any consequences arising from the use of any information it contains.

# Catalytic *n*-pentane Conversion on H-ZSM-5 at High Pressure

Edward P. Schreiner, Shewangizaw Teketel, Raul F. Lobo*

Center for Catalytic Science and Technology
Department of Chemical and Biomolecular Engineering,
University of Delaware, Newark, DE, 19716, USA

*Corresponding Author
Email: lobo@udel.edu
Fax: 302-831-1048
Tel:  302-831-1261

<u>Key Words</u>
Alkane cracking
Endothermic Cooling
Reaction Mechanism
Bronsted Acid Catalysis
Supercritical Fluids

## Abstract

The effect of temperature (633-723 K), pressure (10-60 bar) and weight hourly space velocity (WHSV) (400-1500 $g_{C5}g_{cat}^{-1}h^{-1}$) on the conversion of *n*-pentane on H-[Al]ZSM-5 type catalysts has been investigated. Catalyst properties were tested using a packed-bed laboratory microreactor and reaction products were analyzed via online gas chromatography. 5-25% pentane conversion was observed at a pressure of 40 bar and temperatures in the range of 633-723 K. Reactant consumption rate approached saturation kinetics at pressures above 30 bar (~14% conversion, 673 K). At 40 bar and 673 K, increasing WHSV (400-1500 $g_{C5}g_{cat}^{-1}h^{-1}$) resulted in a reduction in pentane conversion (26-10%). In all cases, propane and butane were the major products, followed by heavier $C_{6+}$ compounds and other lighter products ($C_1$-$C_4$ paraffins and olefins). Propane carbon selectivity increased from 24% at 633 K to 34% at 723 K, while butane carbon selectivity (~40%) was nearly constant. An inverse relationship between the production of $C_{6+}$ and light products was observed with changes in reaction conditions. The carbon selectivity to $C_{6+}$ compounds increased from 20% at 10 bar to 27% at 60 bar and decreased from 28% at 633 K to 18% at 723 K. At all reaction conditions, the observed product distribution can be explained as the result of fast bimolecular reactions, including hydride transfer and alkylation.

## 1. Introduction

This investigation is motivated by the need to develop more efficient cooling technologies for the practical use of new hypersonic engines. The flight of aircraft and missiles at hypersonic speeds (greater than Mach 5) is hindered by overheating of the engine and electronic components caused by the high rate of fuel combustion and air friction[1]. Aircraft are currently cooled by passive and active methods: when passive cooling is used, cold air from the atmosphere is passed through the engine, whereas when active cooling is used, onboard jet fuel is used as a heat sink[2]. In such cases, the maximum amount of heat that can be removed is determined by the heat capacity, thermal stability, and initial temperature of the fuel. Chemical additives (e.g. 1,2,3,4-tetrahydroquinoline and tetralin) and special fuels (e.g. exo-tetrahydrodicyclopentadiene) with greater heat capacity and thermal stability have been designed for this purpose, but future hypersonic vehicles will exceed the cooling capacity of these special fuels[3,4].

Cooling capacity can be improved by utilizing so-called *endothermic fuels*, which undergo endothermic chemical reactions driven by the thermal energy removed from the aircraft[5,6] and a target endothermic reaction is the cracking of hydrocarbons on solid catalysts. For several decades, zeolites have been used as catalysts for cracking of crude oil[7,8], but there are only a few reports of zeolite-based high-pressure cracking for endothermic fuel applications[9–12]. To maximize endothermicity, the selective cracking of alkanes to produce an alkene and a smaller alkane is the preferred reaction. It is also desired to further crack the alkene and alkane to produce hydrogen, ethene, and

methane, as these have better mixing and combustion characteristics than larger molecules[13].

Zeolite catalyzed cracking of alkanes proceeds via two major mechanisms: monomolecular and bimolecular[14]. Monomolecular (i.e. protolytic) cracking reactions typically occur at low pressures and high temperatures[15–21]. In this mechanism, a proton from the zeolite acid site is transferred to the adsorbed alkane to form a pentacoordinated alkanium ion that immediately undergoes protolytic cracking to form a neutral paraffin or molecular hydrogen and a surface alkoxide. The surface alkoxide can desorb to produce an olefin and reform the zeolite acid site.[22–26] This sequence leads to a predictable, but approximate, product distribution. For example, the protolytic cracking of butane can only yield three product pairs: hydrogen and butene, methane and propene, or ethane and ethene. Surface alkoxides can also undergo further cracking through β-scission reactions.

Alkoxides may also participate in bimolecular reactions, such as hydride transfer, oligomerization, and alkylation[8]. In bimolecular reactions, a molecule in the gas phase reacts with a chemisorbed olefin on the surface of the zeolite. The simplest way to detect bimolecular reactions is to observe molecules that cannot be formed from monomolecular cracking; for example, the production of pentane from hexane. Methane and pentene can be produced from protolytic cracking of hexane. Pentene then can be converted to pentane through hydride transfer. Pentane can also be formed by cracking larger molecules that formed through oligomerization.

There have been a few investigations of the supercritical cracking of hydrocarbons on zeolites. Dardas et al. investigated the effects of supercritical

pressures on the conversion and selectivity of *n*-heptane cracking on Y-type zeolites. The supercritical pressures increased the conversion and paraffin yield and decreased the amount of deactivation observed when compared to subcritical pressures[9]. Xian et al. studied supercritical cracking of *n*-dodecane on wall-coated H-[Al]ZSM-5 catalysts and reported that nanocrystalline catalyst particles produced higher conversions and higher selectivity to ethylene and propylene than microcrystal size particles[10]. Kim et al. found that high pressure conversion of methylcyclohexane on H-[Al]ZSM-5 yielded higher heats of reactions as compared to H-[Al]Beta and H-[Al]Y.[27] Luo et al. have investigated the cracking of *n*-hexane on various zeolites. H-[Al]ZSM-5 exhibited a higher pressure dependency on rates and higher activation energies than H-[Al]USY, H-[Al]Mordenite, and H-[Al]Beta, but had better selectivity towards olefins and lower susceptibility to deactivation[11,12]. In addition, the cracking of hexane on ZSM-5 exhibited monomolecular-like reaction kinetics under all pressures, but at high pressures on USY, mordenite, and zeolite beta, bimolecular reactions were the dominant reaction channels. Finally, Wang et al. found that heavily branched *iso*-dodecane (mainly 2,2,4,6,6-pentamethylheptane) could affect conversion of *n*-dodecane on H-[Al]ZSM-5 by acting as an inert dilutent (positive) or by resisting diffusion (negative).[28]

In this report, the effects of temperature, pressure and weight hourly space velocity (WHSV) on the conversion of *n*-pentane on H-[Al]ZSM-5 were investigated to determine the potential of this reaction/catalyst system for endothermic cooling. The solid acid zeolite H-[Al]ZSM-5 was chosen as the catalyst because it is thermally stable, readily available, and known to increase the yield of light olefins in industrial fluidized

4

catalytic cracking units[29]. Pentane was selected because it is the simplest liquid hydrocarbon at STP and has a high cooling potential (pentane cracking to ethane and propylene has a heat of reaction of 1.15 MJ/kg). In addition, *n*-pentane cannot form neutral aromatic species by cyclization and dehydrogenation without molecular weight growth[30]. It was found that under all reaction conditions investigated, bimolecular reactions were the dominant reaction channels for the high-pressure conversion of pentane on H-[Al]ZSM-5. Smaller alkanes ($C_3$, $C_4$) with higher H/C ratios than pentane were produced, while larger species ($C_{6+}$) with lower H/C ratios than pentane were necessarily produced to close the hydrogen and carbon balance. This group of products has lower endothermic potential than direct monomolecular cracking of the alkane.

## 2. Experimental Section

### 2.1 Materials

$NH_4$-[Al]ZSM-5 (CBV3024E) was purchased from Zeolyst International and the material was used without further treatment for the catalytic investigations. *n*-pentane (Fisher, 99.7% purity) was used as the feed for the catalytic tests. The following gases were used for calcination and gas chromatograph operation: Air (Keen, Grade 0.1), Nitrogen (Keen, Grade 5.0), Hydrogen (Keen, Grade 5.0), and Helium (Keen, Grade 5.0).

### 2.2 Characterization

Solid state $^{29}Si$ MAS NMR (99.83 MHz, 10 kHz rotational speed, 2048 scans, and 30 s relaxation delay) and $^{27}Al$ MAS NMR (130.29MHz, 10 kHz rotational speed, and 512 scans) spectra of hydrated $NH_4$-[Al]ZSM-5 were recorded with a Bruker AVIII500 NMR spectrometer. Surface area and micropore volumes (calculated using the t-plot

5

method) were determined through $N_2$ adsorption isotherms measured using a

Micromeritics ASAP 2020 instrument. The samples were pretreated at a temperature of

623 K and a reduced pressure of 0.5 torr for 6 h to remove any adsorbed species.

Powder X-ray diffraction patterns (PXRD) were measured using a Phillips X'Pert X-ray

diffractometer with a CuKα source (λ = 1.542 Å). Diffraction patterns were obtained

using a step size of 0.02° 2Θ with 2 s counting time at each step. Diffraction patterns

were measured between 5° and 50° 2Θ. SEM images were taken with a JSM-7400F

scanning electron microscope with an accelerating voltage of 3.00 kV. Zeolite chemical

compositions were determined through inductively coupled plasma mass spectrometry

(ICP-MS) from Galbraith Laboratories, Inc.

### 2.3 Reactor system

**Figure 1: Process flow diagram of the experimental setup
used for high pressure experiments**

Figure 1 depicts the configuration of the experimental setup used for high-

pressure experiments. The reactant, *n*-pentane, was contained in a pressurized tank (1

L); this limited amount constrained the time on stream to under 9 h.  Pentane was fed

into the system using a high-pressure liquid chromatography (HPLC) pump (Chromtech,

Series I). The system pressure was controlled by a backpressure regulator (Swagelok,

KPB series). The reactor consisted of the catalyst supported by quartz wool inside a

316 SS tube (4.6 mm ID). Two thermocouples were installed, one at the bottom and one

at the top of the catalyst bed, to monitor the temperature difference across the bed; the

thermocouples also helped maintain the position of the bed within the reactor tube. A

preheater (coiled 1/8" tube wrapped with heating tape) and tubular furnace (Lindberg

6

Blue M) were used to control the reaction temperature. Gas transfer lines were heated to 453 K using heating tape to avoid condensation of products. The reactor effluent was analyzed using an online gas chromatograph (GC) (Agilent 7890B) equipped with a flame ionization detector (FID). Separation of chemical species within the reactor effluent was performed in the GC with an Alumina column (Agilent, 50 m x 530 µm ID). Helium was used as the carrier gas and nitrogen was used as the makeup gas. The following temperature program was used for product detection: a 5 minute hold at 373 K, a ramp to 473 K at a rate of 20 K/min, and a final 30 min hold at 473 K.

## 2.4 Catalytic tests

The catalyst powder was pressed, gently crushed and sieved to particle sizes between 250 and 425 µm (40 – 60 mesh). Each experiment was performed using 50 mg of catalyst powder. Prior to each experiment, the catalyst was calcined *in situ* at a temperature of 823 K for 5 hours in zero air (Keen, 60 mL/min). A variety of reaction conditions were investigated: pressure was investigated up to 60 bar and reaction temperature was studied in the range of 633 – 723 K. Most experiments were performed in the supercritical regime of *n*-pentane ($t_c$ = 470 K and $p_c$ = 34 bar)[31]. The weight hourly space velocity (WHSV, defined as grams of pentane fed per gram of catalyst per hour) ranged from 375 – 1500 $g_{C5}g_{cat}^{-1}h^{-1}$ and was controlled by changing the pentane liquid flow rates in the range of 0.5 - 2.0 mL/min. Conversion of *n*-pentane was defined as 100% minus the percentage of unreacted pentane (all isomers included) in the product stream. Product carbon selectivity was defined as the fraction of carbon in each product as compared to the total amount of carbon in the effluent that was not pentane.

7

## 3. Results

The conversion of *n*-pentane over zeolite H-[Al]ZSM-5 (Si/Al = 15) was investigated considering the effect of temperature (633-723 K), pressure (10-60 bar), and weight hourly space velocity (WHSV) (375-1500 $g_{C5}g_{cat}^{-1}h^{-1}$). The reaction kinetics were measured using a packed-bed laboratory microreactor and reaction products were analyzed via online gas chromatography.

### 3.1 Catalyst characterization

The XRD patterns of the zeolite samples showed that the zeolite samples were highly crystalline and did not reveal the presence of any amorphous material or other crystalline impurities. The SEM image (Figure 2) shows that the material was an aggregate of particles smaller than 2 µm. Presence of only one signal at 55 ppm on the $^{27}Al$ MAS NMR spectra of the hydrated samples showed that nearly all aluminum atoms were in tetrahedral coordination (Figure 2). Only a small fraction (1%) was observed near 0 ppm and was assigned to extra-framework octahedral aluminum. The nominal Si/Al ratio of this commercial sample determined by ICP (Si/Al = 15.7) was consistent with the aluminum concentrations determined by other studies on similar samples (Si/Al = 15-17)[15,32]. $^{29}Si$ MAS NMR spectra from this sample indicated that the sample contained predominantly Si(4Si) groups and 4.2% of Si(3Si, Al), resulting in an estimated framework Si/Al of 23. The aluminum concentration is slightly less than the amount observed by ICP, and confirms that only a small fraction of the Al is located in extra-framework positions.

The micropore volume, obtained from $N_2$ adsorption isotherms and analyzed using the t-plot method, was 0.11 $cm^3/g$. This micropore volume is slightly smaller than

observed for high quality samples (usually ~0.14 $cm^3/g$) and suggest that some extra-

framework species may be present in the zeolite pores or that a non-porous phase

(undetected by XRD) is present in the sample. The observed BET surface area (380

$m^2/g$) and micropore volume are in agreement with previous reports for the same

material[32].

**Figure 2: SEM image of CBV3024E (*top*), $^{29}$Si NMR (*left*), and $^{27}$Al NMR (*right*) of the ZSM-5 catalyst.**

### 3.2 Catalytic conversion of *n*-pentane

Conversion of *n*-pentane on H-[Al]ZSM-5 at high pressures was performed in a

packed-bed reactor. Reactor effluent was analyzed via an online GC with injections

being taken approximately every 40 min. As seen in Figure 3, reactor conversion

remained stable during the 6 h of time on stream at temperatures up to 673 K.

Deactivation was observed at temperatures above 673 K, with the greatest amount at

the highest reaction temperature of 723 K. Conversion and selectivity data were

calculated from the average of the GC measurements over the 6.5 h time on stream.

**Figure 3: Conversion of *n*-pentane over 6.5 h time on stream during high pressure conversion on H-[Al]ZSM-5. Reaction conditions: T = 633 – 723 K, P = 40 bar, and WHSV = 1120 $g_{C5}g_{cat}^{-1}h^{-1}$**

Figure 4 shows the conversion of *n*-pentane and product carbon selectivity at

temperatures between 633 K and 723 K (P = 40 bar and WHSV of 1120 $g_{C5}g_{cat}^{-1}h^{-1}$).

9

Conversion increased rapidly with increasing temperature. The major products of the reaction were propane and butane (~6:4 *n:iso* isomeric ratio). At all experimental conditions investigated, the selectivity to methane, ethane, ethene, propene and butenes was low (<10%), hence these fractions were combined and reported as 'lights'. This fraction never exceeded 10% of the overall carbon in the product stream. A typical carbon composition of the lights was 1% methane, 5-10% ethane, 4-8% ethylene, 20-30% propylene, and 50-70% butenes. As temperature increased, selectivity to propane increased, while selectivity to butane remained nearly constant. On the other hand, selectivity to higher molecular weight products ($C_{6+}$) decreased with increasing temperature. A small (<2%) increase in selectivity to light products was observed with increasing temperature.

**Figure 4: Conversion of *n*-pentane (*left*) and selectivity to product groups (*right*) during high pressure conversion on H-[Al]ZSM-5. Reaction conditions: T = 633 – 723 K, P = 40 bar, and WHSV = 1120 $g_{C5}g_{cat}^{-1}h^{-1}$**

Clear changes in conversion and carbon selectivity were observed as the pressure was increased at a temperature of 673 K and WHSV = 1120 $g_{C5}g_{cat}^{-1}h^{-1}$. Increasing the pressure of the system from 10 bar up to a total pressure of 30 bar, which is before the transition to the supercritical phase (34 bar), caused an increase in conversion. Further increases in pressure up to 60 bar did not increase the total conversion of pentane. Pressure changes had little effect on carbon selectivity of the major products: propane and butane. Conversely, increases in pressure decreased selectivity to the light products and increased selectivity to the $C_{6+}$ fraction.

**Figure 5: Conversion of *n*-pentane (*left*) and selectivity to product groups (*right*) during high pressure conversion on H-[Al]ZSM-5. Reaction conditions: T = 673 K, P = 10 - 60 bar, and WHSV = 1120 $g_{C5}g_{cat}^{-1}h^{-1}$**

Figure 6 shows the conversion and carbon selectivity during the *n*-pentane reaction at a temperature of 673 K and a pressure of 40 bar as a function of WHSV (375 – 1500 $g_{C5}g_{cat}^{-1}h^{-1}$). Conversion of pentane increased with decreasing WHSV, or in other words, increased as the residence time increased. Selectivity of the major products (propane and butane) and $C_{6+}$ fraction did not change appreciably with changes in WHSV, but carbon selectivity of the light products increased with increasing WHSV.

**Figure 6: Conversion of *n*-pentane (*left*) and selectivity to product groups (*right*) during high pressure conversion on H-[Al]ZSM-5. Reaction conditions: T = 673 K, P = 40 bar, and WHSV = 375 -1500 $g_{C5}g_{cat}^{-1}h^{-1}$**

## 4. Discussion

The formation of more than 50 different species upon the reaction of *n*-pentane on H-[Al]ZSM-5, including many compounds heavier than pentane, is clear evidence of secondary bimolecular reactions controlling the product distribution at high pressure. In addition, the ratios of $C_3/C_2$ and $C_4/C_1$ products were greater than 1 under all conditions, which further indicates a role of bimolecular reactions in the catalyst. If monomolecular cracking were occurring, the average H/C ratio of the cracked products would equal that of the feed (*n*-pentane H/C = 2.4), while the average H/C of products lighter than pentane was between 2.5 – 2.6. Since the observed $C_1$-$C_5$ species had an average H/C greater than the feed, either the olefins produced from monomolecular cracking were

consumed in secondary reactions or the paraffins were produced via a reaction other

than *n*-pentane cracking.

The consumption of olefins lighter than pentane through secondary bimolecular

reactions is consistent with changes in the carbon selectivity of the light olefins: ethene,

propene, and butene (Figure 7). Carbon selectivity of the light olefins decreased with

increasing pressure, with the change being most clear at pressures below ~ 30 bar,

where pentane is gas-like. Although pentane conversion did not change above 30 bar,

product selectivity continued to change with increasing pressure. Elevated pressures

promote oligomerization of olefins[33–35], a reaction also observed here. Increasing

pressure decreased light olefin production and increased formation of $C_{6+}$ compounds.

Although elevated pressures promote oligomerization, the larger compounds in the $C_{6+}$

fraction eventually become more reactive and crack at high temperatures as seen in

Figure 4. As reaction temperature increases, cracking rates of the $C_{6+}$ fraction become

greater than oligomerization rates, leading to an increase in the production of propane.

Carbon selectivity of the light olefins also increased with increasing WHSV. With less

time to react, a greater percentage of light olefins formed through monomolecular

cracking of pentane survived without undergoing further bimolecular reactions. From the

observed trends in carbon selectivity of the light olefins, a simplified reaction network

can be proposed to illustrate the formation of the major products: propane and butane.

**Figure 7: Selectivity of products within the lights fraction at various temperatures (*left*), pressures (*middle*), and WHSV (*right*). Reaction conditions: T = 633 - 723 K, P = 10 - 60 bar, and WHSV = 375 -1500 $g_{C5}g_{cat}^{-1}h^{-1}$**

12

Figure 8 displays a simplified reaction network consistent with the observed formation of propane and butane. After protolytic cracking of *n*-pentane, propene and ethane are formed and the propene then can react with another pentane via hydride transfer. This forms one of the major products, propane. The pentene can crack via beta scission to form another molecule of propene and ethene. Any ethene that is formed can dimerize to form butene. The butene can react with another pentane via hydride transfer yielding the second major product, butane. Through oligomerization, compounds heavier than pentane can form and subsequently crack to form lighter products or cyclize and aromatize. In reality, a more complex reaction network of monomolecular and bimolecular reactions exists, as evidenced by the product distribution and trends in activation energy.

**Figure 8: Simplified reaction network demonstrating the production of propane and butane**

If monomolecular cracking were the dominant reaction channel, as pressure increases, the apparent activation energy should also increase and approach the intrinsic activation energy. This trend occurs because saturation kinetics are reached at elevated pressures, reducing the effect of adsorption enthalpy on the apparent activation energy [11]. As seen in Figure 9, the apparent activation energy based on consumption of *n*-pentane decreases with increasing pressure, which is opposite of the expected trend for monomolecular cracking. Furthermore, Luo et al. reported the intrinsic activation energy of *n*-hexane cracking on ZSM-5 to be 170 kJ/mol, while Gounder et al. reported the intrinsic activation energy of propane cracking on ZSM-5 to

13

be 204 kJ/mol[11,15]. Based on these observations, it is expected that the activation

energy above the saturation pressure of *n*-pentane (>30 bar) to be near those of

propane and hexane[15]. At 40 bar, the apparent activation energy for the consumption of

*n*-pentane was 86 kJ/mol, which was much less than expected for monomolecular

cracking, but consistent with the results obtained using other zeolite frameworks as

solid acid catalysts.

**Figure 9: Activation energies at 10 bar (*square*), 20 bar (*circle*), and 40 bar (*triangle*). Reaction conditions: T = 633 - 673 K, P = 10 - 40 bar, and WHSV = 1120 $g_{C5}g_{cat}^{-1}h^{-1}$**

Luo et al. recently investigated the high pressure cracking of *n*-hexane on H-

USY, H-Beta, and H-Mordenite. In the work, the apparent activation energy for cracking

on zeolite beta (63 kJ/mol) and USY (55 kJ/mol) did not change with pressure, while the

apparent activation energy on mordenite decreased from 77 kJ/mol at 1 bar to 66

kJ/mol at 137 bar[12]. The activation energies observed from the cracking of hexane on

USY, zeolite beta, and mordenite are consistent with those for the cracking of *n*-pentane

on ZSM-5, but differ from the cracking of *n*-hexane on ZSM-5.

Luo et al. also investigated the product selectivity for the cracking of *n*-hexane on

ZSM-5[12]. With increasing conversion under isothermal conditions, an increase in

selectivity to higher molecular weight species was observed. For the conversion of *n*-

pentane on ZSM-5, increasing conversion under isothermal conditions did not result in

any significant change in selectivity to higher molecular weight species. However, there

were two trends in product selectivity that were similar between the conversion of

pentane and hexane on ZSM-5. First, the major products of hexane conversion were

butanes and pentanes, analogous to propane and butanes for pentane conversion.

14

Second, increasing pressure caused a decrease in selectivity to light olefins for the conversion of both pentane and hexane on ZSM-5.

The decrease in activation energy with increasing pressure is evidence of a shift from a higher activation energy reaction channel to a lower activation energy reaction channel. While the conversion of pentane and hexane on ZSM-5 have similar trends in product selectivity with changing pressure, the differences in apparent activation energy suggest the conversion occurs via alternative reaction pathways.

## 5. Conclusions

The high selectivity (>70%) to propane and butane, along with the observed changes in the selectivity to lights and $C_{6+}$ compounds, indicate that bimolecular reactions, such as hydride transfer and alkylation, control product distribution. While the product distribution from the high pressure conversion of pentane resulted in an endothermic process, hydride transfer reactions led to the transformation of high energy olefins into lower energy paraffins and aromatics, resulting in a decrease of the process endothermicity from a target of 1.1 MJ/kg of *n*-pentane converted to an estimated 0.6 MJ/kg. Hydride transfer occurs readily on H-[Al]ZSM-5 and other zeolites, and an alternative catalyst that suppresses these reactions should improve selectivity to light olefins, which will increase cooling capacity of the endothermic fuel.

## Acknowledgements

## References

1    H. Lander and A. C. Nixon, *J. Aircr.*, 1971, **8**, 200–207.

2    *US Pat.,* US 2012/0305712 A1, 2012.

3    T. J. Bruno and J. A. Widegren, *Energy and Fuels*, 2009, **23**, 5523–5528.

4    H. S. Chung, G. S. H. Chen, R. a. Kremer, J. R. Boulton and G. W. Burdette, *Energy and Fuels*, 1999, **13**, 641–649.

5    N. Gascoin, G. Abraham and P. Gillard, *J. Anal. Appl. Pyrolysis*, 2010, **89**, 294–306.

6    J. Kim, D. H. Hyeon, S. H. Park, B. H. Chun, B. H. Jeong, J. S. Han and S. H. Kim, *Catal. Today*, 2014, **232**, 63–68.

7    M. Stöcker, *Microporous Mesoporous Mater.*, 2005, **82**, 257–292.

8    A. Corma, *Chem. Rev. (Washington, D C )*, 1995, **95**, 559–614.

9    Z. Dardas, M. G. Suer, Y. H. Ma and W. R. Moser, *J. Catal.*, 1996, **159**, 204–211.

10   X. Xian, G. Liu, X. Zhang, L. Wang and Z. Mi, *Chem. Eng. Sci.*, 2010, **65**, 5588–5604.

11   J. Luo and R. J. Gorte, *Catal. Letters*, 2013, **143**, 313–316.

12   J. Luo, B. V. Bhaskar, Y. H. Yeh and R. J. Gorte, *Appl. Catal. A Gen.*, 2014, **478**, 228–233.

13   W. Ning, P. Yu and Z. Jin, *Proc. Inst. Mech. Eng. Part G J. Aerosp. Eng.*, 2012, **227**, 1780–1794.

14   W. O. Haag and R. M. Dessau, *Duality of Mechanism for Acid-Catalyzed Paraffin Cracking*, Princeton, NJ, 1985.

15   R. Gounder and E. Iglesia, *J. Am. Chem. Soc.*, 2009, **131**, 1958–1971.

16   S. M. Babitz, B. a. Williams, J. T. Miller, R. Q. Snurr, W. O. Haag and H. . Kung, *Appl. Catal. A Gen.*, 1999, **179**, 71–86.

17   T. F. Narbeshuber, H. Vinek and J. A. Lercher, *J. Catal.*, 1995, **157**, 388–395.

18   A. Janda and A. T. Bell, *J. Am. Chem. Soc.*, 2013, **135**, 19193–19207.

19   A. Bhan, R. Gounder, J. Macht and E. Iglesia, *J. Catal.*, 2008, **253**, 221–224.

20   B. Xu, C. Sievers, S. B. Hong, R. Prins and J. A. van Bokhoven, *J. Catal.*, 2006, **244**, 163–168.

21   M. Derewinski and F. Fajula, *Appl. Catal. A Gen.*, 1994, **108**, 53–61.

16

22    V. B. Kazansky, *Catal. Today*, 1999, **51**, 419–434.

23    A. Corma, P. J. Miguel and A. V. Orchilles, *J. Catal.*, 1994, **145**, 171–180.

24    T. F. Narbeshuber, A. Brait, K. Seshan and J. A. Lercher, *J. Catal.*, 1997, **136**, 127–136.

25    J. H. Yun and R. F. Lobo, *J. Catal.*, 2014, **312**, 263–270.

26    J. H. Yun and R. F. Lobo, *Catal. Sci. Technol.*, 2015, **5**, 264–273.

27    J. Kim, S. H. Park, B. H. Chun, B. H. Jeong, J. S. Han and S. H. Kim, *Catal. Today*, 2012, **185**, 47–53.

28    Y. Wang, X. Xian, X. Hou, X. Zhang, L. Wang and G. Liu, *J. Anal. Appl. Pyrolysis*, 2014, **113**, 133–136.

29    A. Farshi and H. R. Abri, *Pet. Sci. Technol.*, 2012, **30**, 1285–1295.

30    E. V. Anslyn and D. A. Dougherty, *Modern Physical Organic Chemistry*, University Science Books, 2006.

31    D. J. Rosenthal and A. S. Teja, *AICHE J.*, 1989, **35**, 1829–1834.

32    J. C. Groen, J. A. Moulijn and J. Pérez-Ramírez, *Ind. Eng. Chem. Res.*, 2007, **46**, 4193–4201.

33    R. Quann, L. Green, S. A. Tabak and F. J. Krambeck, *Ind. Eng. Chem. Res.*, 1988, **27**, 565–570.

34    B. Chiche, E. Sauvage, F. Di Renzo, I. I. Ivanova and F. Fajula, *J. Mol. Catal. A Chem.*, 1998, **134**, 145–157.

35    C. Bertrand-Drira, X. Cheng, T. Cacciaguerra, P. Trens, G. Melinte, O. Ersen, D. Minoux, A. Finiels, F. Fajula and C. Gerardin, *Microporous Mesoporous Mater.*, 2015, **213**, 142–149.
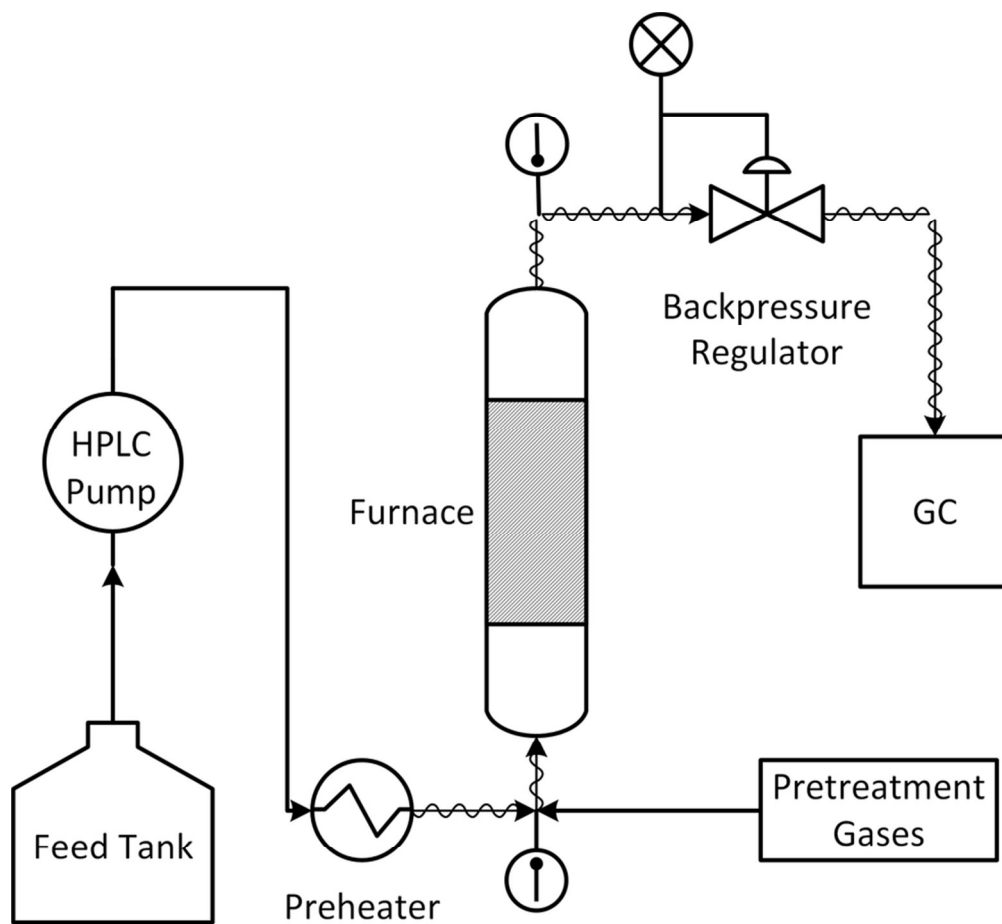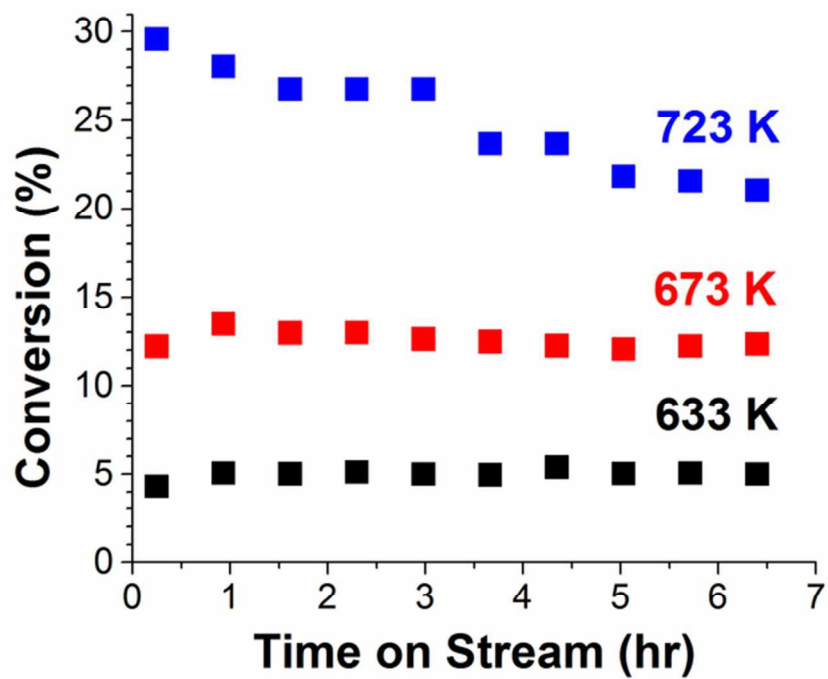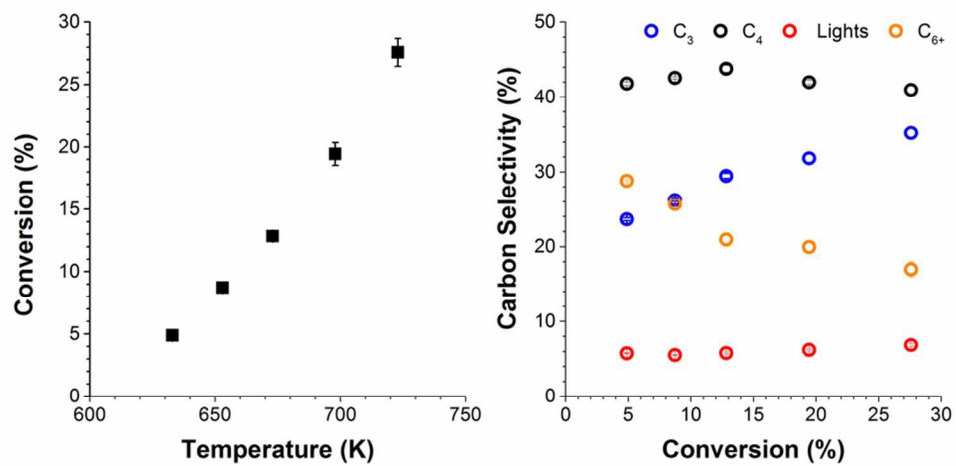
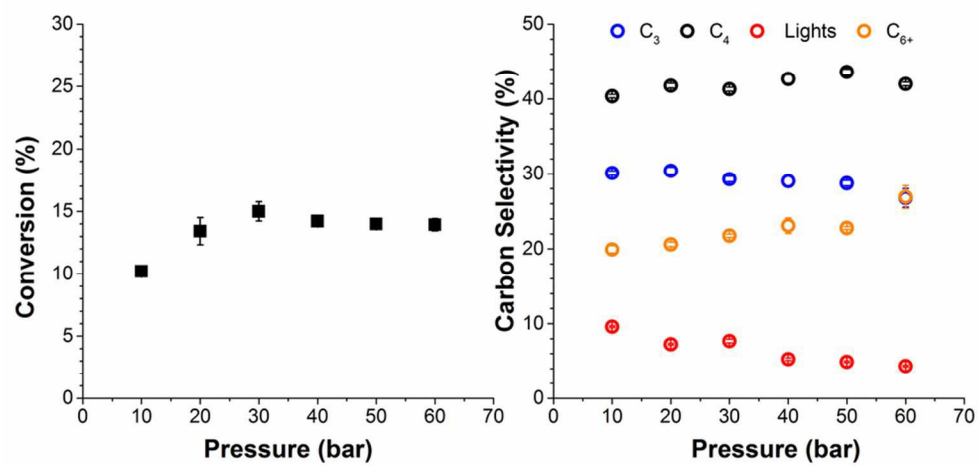82x77mm (300 x 300 DPI)
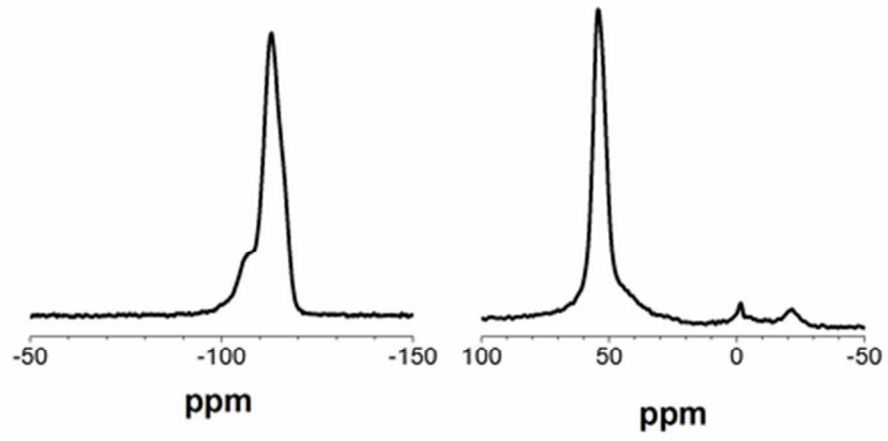
41x20mm (300 x 300 DPI)
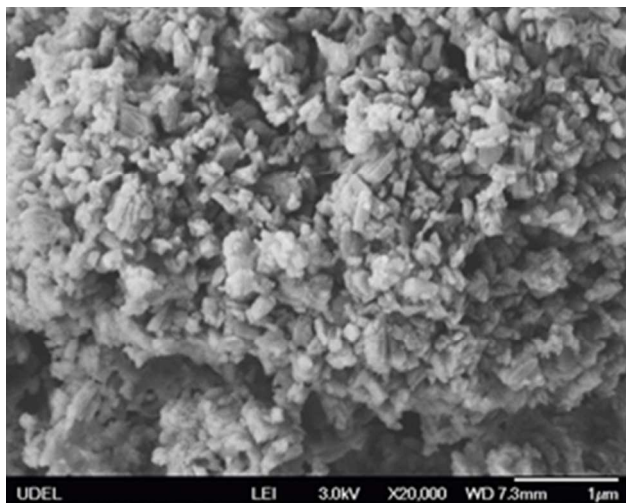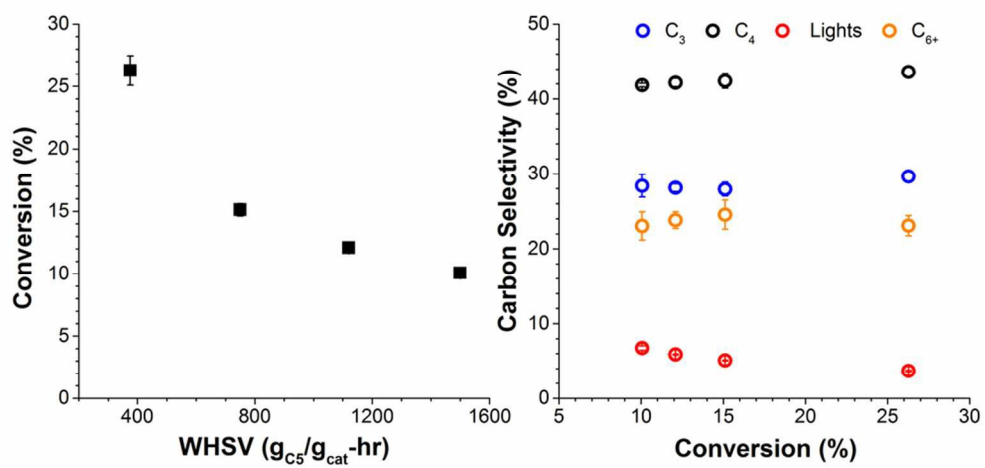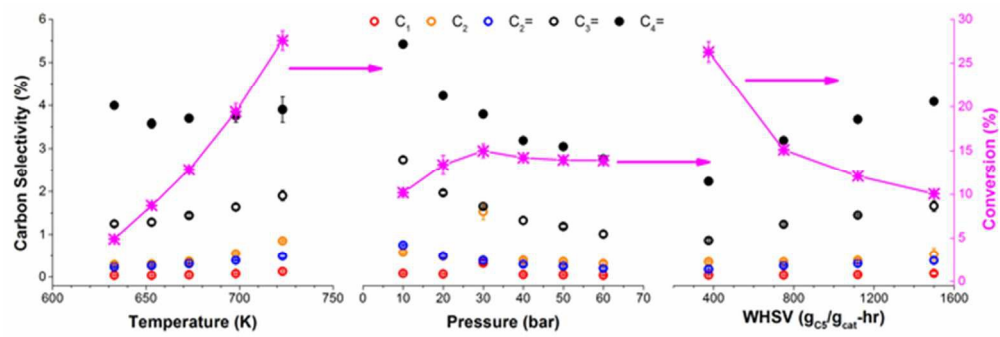
82x65mm (96 x 96 DPI)

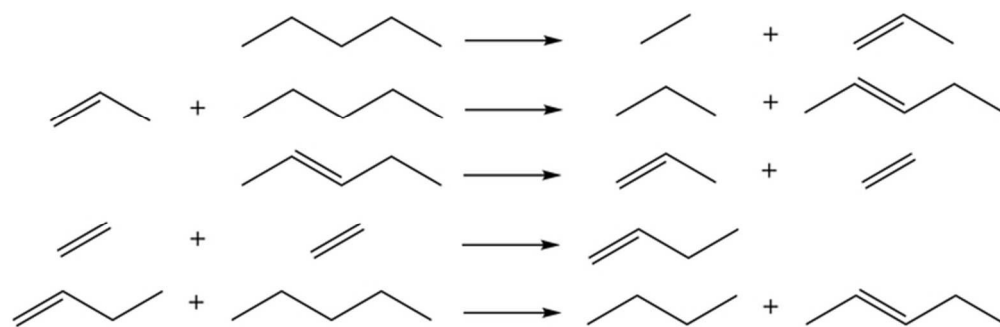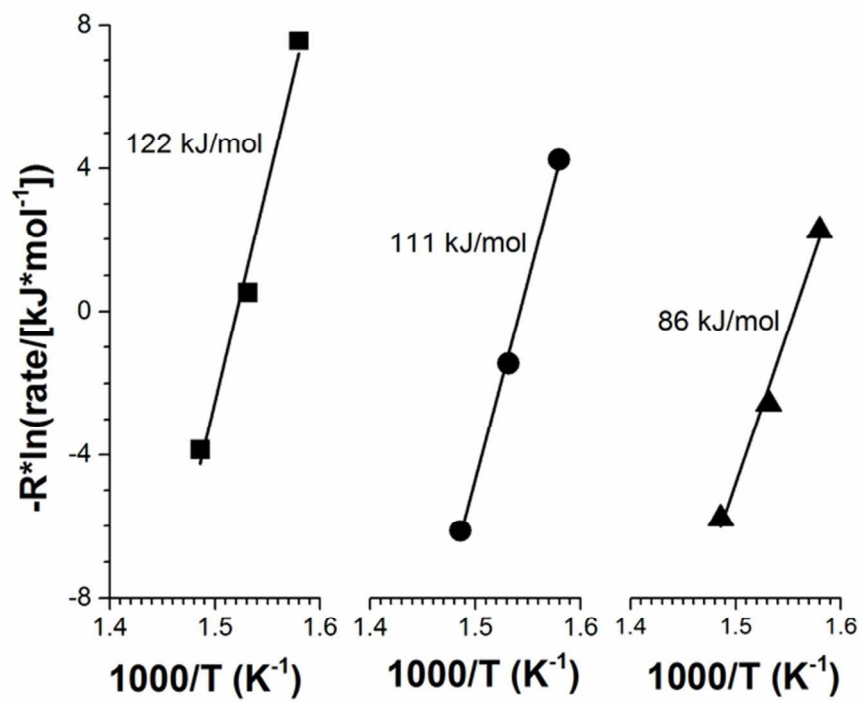63x48mm (300 x 300 DPI)

85x42mm (300 x 300 DPI)
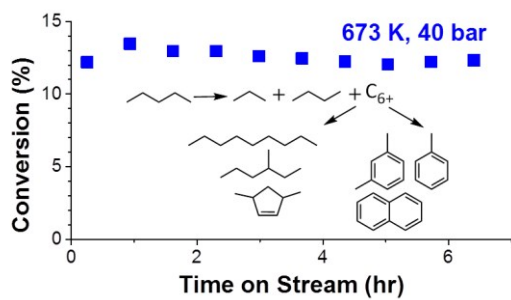
85x42mm (300 x 300 DPI)

85x42mm (300 x 300 DPI)

56x18mm (300 x 300 DPI)

59x19mm (300 x 300 DPI)

63x48mm (300 x 300 DPI)

**New Journal of Chemistry**



Highly stable, high pressure *n*-pentane conversion on H-[Al]ZSM-5 yields $C_3$ and $C_4$ alkanes and heavier hydrocarbons to balance H/C ratio.